NANO LETTERS

2006
Vol. 6, No. 8
1711−1718

Probing the Electronic Properties of Self-Organized Poly(3-dodecylthiophene) Monolayers by Two-Dimensional Scanning Tunneling Spectroscopy Imaging at the Single Chain Scale

Lorette Scifo,[†] Mathieu Dubois,[†] Mickaël Brun,[‡] Patrice Rannou,[†] Sylvain Latil,[§] Angel Rubio,[||,⊥] and Benjamin Grévin*,[†]

UMR5819 (CEA-CNRS-Université Grenoble I), CEA/DRFMC/SPrAM/LEMOH, 17 rue des Martyrs, 38054 Grenoble Cedex 9, France, CEA-Grenoble LETI/DIHS/LMNO, 17 rue des Martyrs, 38054 Grenoble Cedex 9, France, Laboratoire de Physique du Solide, FUNDP, 61 rue de Bruxelles, B-5000 Namur, Belgium, Institut für Theoretische Physik, Freie Universität Berlin, Arnimallee 14, D-14195 Berlin, Germany, and European Theoretical Spectroscopy Facility (ETSF) and Departamento Fìsica de Materiales, Facultad de Quìmicas, Universidad del Paìs Vasco, Centro Mixto CSIC-UPV/EHU and Donostia International Physics Center (DIPC), 20018 San Sebastian, Spain

Received May 5, 2006; Revised Manuscript Received June 21, 2006

ABSTRACT

Regioregular poly(3-dodecylthiophene) films self-organized on highly oriented pyrolytic graphite have been investigated by scanning tunneling microscopy and two-dimensional scanning tunneling spectroscopy (STS). Simulated spectra in very good agreement with the experimental data have been obtained by a method combining ab initio and semiempirical approaches, which allows a careful discussion of the polymer electronic states. From the experimental data, with the support of modeling, it is shown that the STS spectra give a direct access to the polymer semiconducting band gap without noticeable charge-transfer effects from the substrate. Spectroscopic images are achieved at the single chain scale, which allows scrutinizing the electronic consequences of chain folds and π-stacking effects through spectroscopic contrasts. While chain folds do not locally increase the polymer band gap more than a few tens of millielectonvolt, a striking widening of the STS conductance gap is observed in the case of electronic tunneling through two interacting polymer layers. Scenarios based on nonplanar configuration of thiophene cycles within the second layer or variations of the charge screening effects are proposed to explain this phenomenon.

Controlling the self-organization and electronic properties of molecular and macromolecular systems on surfaces is among the most challenging quests of molecular and organic electronics. To date, scanning tunneling microscopy (STM) and its spectroscopic mode (STS), giving access to molecular conformation and electronic states, have been major tools to study various molecular systems such as porphyrins,[1−3] phthalocyanines,[4] Lander molecules,[5] π-conjugated oligomers,[6−8] C_{60},[9−13] or carbon nanotubes.[14−16]

These past years, π-conjugated macromolecular systems have also emerged as a new class of materials which can present both self-assembly and novel electronic features. Especially, some self-organized semiconducting polymers constitute model systems for the realization of π-conjugated molecular nanowires[17−22] and for fundamental STM investigations on surfaces.

For regioregular polythiophenes, which stand as generic models owing to their remarkable semicrystalline properties[23,24] and resulting high carrier mobilities in organic field effect transistors,[25,26] there is still a crucial need to determine, at the local scale, the precise relationship between structural organization and electronic properties.

Recent studies on polydiacetylene nanowires,[19,20] on electrochemically polymerized poly(thiophene)s on I−Au(111),[21,22] and on isolated poly(3-hexylthiophene) (P3HT) chains randomly dispersed by the pulsed valve technique on H-terminated silicon[27−29] have shown that the electronic

* Corresponding author. E-mail: benjamin.grevin@cea.fr.
[†] UMR5819 SPrAM.
[‡] CEA-Grenoble LETI.
[§] FUNDP.
[||] Freie Univversität, Berlin.
[⊥] Universidad del Paìs Vasco.

10.1021/nl061018w CCC: $33.50
Published on Web 07/25/2006

properties of π-conjugated polymer submonolayer films can be locally investigated by STS.[19,20,22,28,29]

Besides the analysis of the polymer local density of states, the simultaneous acquisition of STM topographic and two-dimensional (2D) spectroscopic images should allow, in principle, investigation of the impact of the polymer local conformation on its electronic properties. However, to our knowledge, two-dimensional spectroscopic images resolved at the single chain scale have only been obtained[28,29] by Terada et al. for P3HT on H−Si(100). Moreover, on this surface, neither packing features nor self-assembly mechanisms were obtained for P3HT,[27] which does not promote STS imaging of local electronic contrast on well-resolved conformational features.

In this Letter, we use poly(3-dodecylthiophene) (P3DDT) 2D polycrystals on highly oriented pyrolytic graphite (HOPG),[30,31] as model systems for STM and STS investigations of the local electronic properties of self-organized π-conjugated polymer chains. We go beyond previous STM studies on self-organized poly(3-alkylthiophene)s by performing two-dimensional STS imaging investigations of electronic properties on self-organized chains with perfectly defined conformations (rodlike, folded chains), with the support of theoretical calculations combining ab initio with semiempirical approaches.

Following this modeling scheme, a clear assignment of the most prominent STS features to the contributing molecular states is achieved. This allows a careful discussion of the polymer electronic states, and the calculations definitely confirm the relation between the STS conductance gap and the polymer band gap. We also explain why there are no significant charge-transfer effects between P3DDT chains and the HOPG substrate. By a proper positioning of molecular levels within the tunneling junction, and by taking into account electronic correlations, simulated spectra are obtained in very good agreement with the experimental data. The apparent gap reduction displayed by STS spectra, in comparison to measurements in solution, is then shown to arise from extrinsic charge screening effects in the tunneling junction.

Then, by analyzing the local polymer band gap variation throughout 2D STS images, we especially address the question of the impact of chain folding on the local polymer band gap and show that its increase is limited to a few tens of millielectonvolt. Moreover, the presence of isolated chains of a second layer[30] opens the possibility to analyze the superimposed contribution of interchain $\pi-\pi$ electronic coupling on the STS spectra and images, and a striking widening of the effective conductance gap over the second layer is revealed and discussed in the frame of scenarios based on conformational defects within the second layer and variations of the charge screening effects.

P3DDT films with submonolayer coverage were prepared by drop-casting from $CHCl_3$ solution (with an optical gap of 2.2 ± 0.1 eV measured in THF solution by UV−vis spectroscopy) as described in ref 31. STM experiments were performed in the low-current mode, at room temperature, under ultrahigh-vacuum conditions (base pressure below 5×10^{-11} mbar), using a VT Omicron system and PtIr tips. We underline that in this setup, the bias voltage V_g is applied to the tip and the sample is grounded. Spectroscopic data were acquired in the current imaging tunneling spectroscopy mode (CITS) in which topographic images, in the constant current mode, are recorded simultaneously with $I-V$ curves taken on a grid, the feedback loop being disabled during spectroscopic acquisition. Conductance spectra dI/dV were recorded using a lock-in technique. Normalization ((dI/dV)/(I/V) curves) was performed afterward, an adequate small constant being added to (I/V) to prevent excessive noise within the band gap.[32] To improve the signal over noise ratio, spectra were averaged over several adjacent pixels on current images, and the related spectroscopic images were filtered (except Figure 3b) by a smooth Gaussian function. Nontreated spectroscopic data display the same features with a slightly higher noise level.

A typical topographic STM image of a submonolayer P3DDT film on HOPG is presented in Figure 1a. It displays a highly organized 2D polycrystalline structure with 3-fold oriented monodomains connected by well-defined regular, 120° or 60° chain folds.[33] This supramolecular organization is induced by the strong epitaxy of lateral alkyl chains on HOPG, which promotes the formation of single monolayers and induces a full interdigitation of rodlike chains within the monodomains. However, a second layer is also occasionally observed,[30] featuring isolated polymer chains, labeled P2 chains from hereon **(**P1 will refer to the first layer**)**. Most of P2 chains seem randomly oriented, a majority of them crossing the underlying P1 chains. This raises the question of the presence of intrachain defects within P2 backbones, which may affect the overlap of thiophene cycles π-orbitals with a direct effect on the stacking height between the two layers. The analysis of 20 z-histograms based on STM images taken at $V_g = 1.4$ V (inset on Figure 1b) leads to heights of $h_{P1-HOPG} = 0.24 \pm 0.04$ nm and $h_{P2-P1} = 0.29 \pm 0.05$ nm for P1 on HOPG and P2 on P1, respectively. Both values are lower than the ones generally expected for π-conjugated cycles on HOPG **(**in the 0.35−0.38 nm range**)** and π-stacked thiophene cycles (0.38 nm for bulk P3ATs), indicating nonnegligible electronic contributions. It is likely that the observed difference between $h_{P1-HOPG}$ and h_{P2-P1} results from a variation of electronic properties above the two layers, with a greater electronic density above P2 compensated by an increased tip−sample distance. An enhanced electronic delocalization assisted by π-stacking could be invoked, which precludes, however, the existence of strong structural disorder within P2 backbones. STM z-images contrasts induced by inhomogeneous electronic density might also be expected when considering chains of different length or chain folds. Nevertheless, for both features, no specific contrast is observed on topographic images with $1 \text{ V} \leq V_g \leq 1.4$ V. To address all these questions, a deeper analysis of the electronic states through $I-V$ curves and their derivatives is required and will be presented hereafter. For such STS investigations on π-conjugated polymers, the use of the low-current mode[31] is a critical asset as it enables a very stable tunneling junction, as shown by Figure 1c,d, thus enhancing the quality of CITS data.

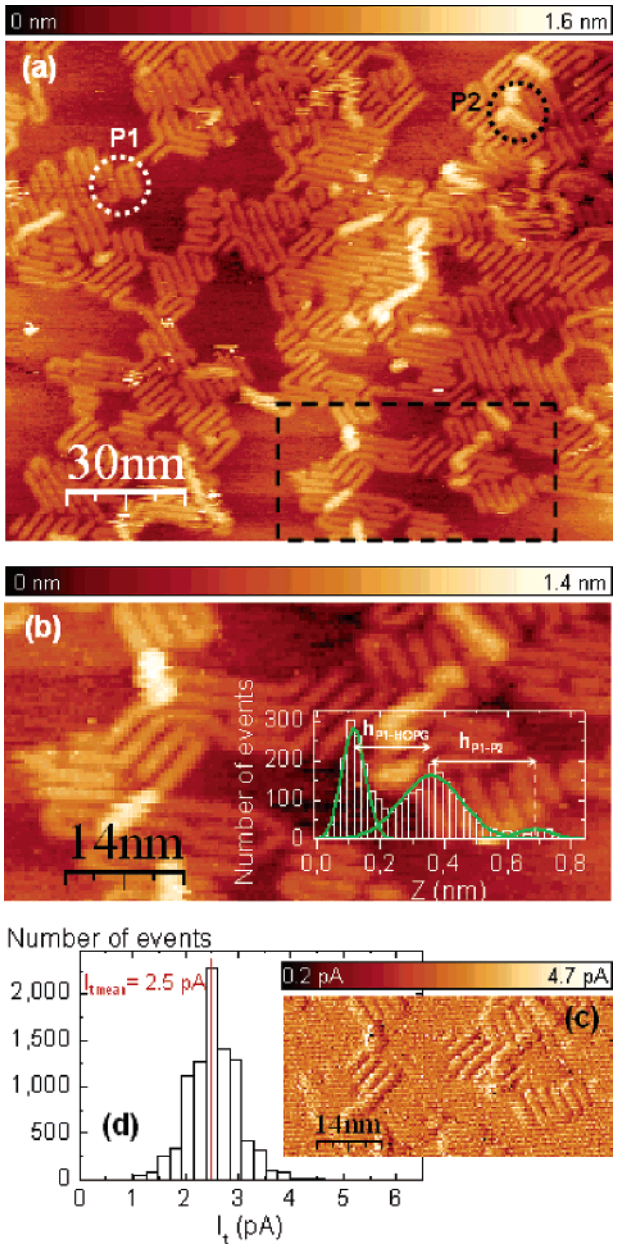

Figure 1. STM images of a P3DDT film on HOPG with submonolayer coverage obtained in the low-current mode**.** Set-point values $I_t = 2.5$ pA, $V_g = 1.4$ V. (a) Topographic image (150 nm × 123 nm, pitch = 0.5 nm). The white and black dotted circles highlight the first polymer layer and the partially nucleated second layer, respectively. (b) Magnified view of the area (68 nm × 34 nm) indicated by the dotted square on (a). Determination of monolayer and bilayer stacking heights from *z*-histograms (see text). (c) Current image recorded simultaneously with the topographic *z*-values of image (b). The slight background current modulation is generated by the bias modulation applied with the lock-in amplifier. (d) Corresponding current histogram. These results demonstrate that low currents are very well regulated on both the monolayer and the second layer.

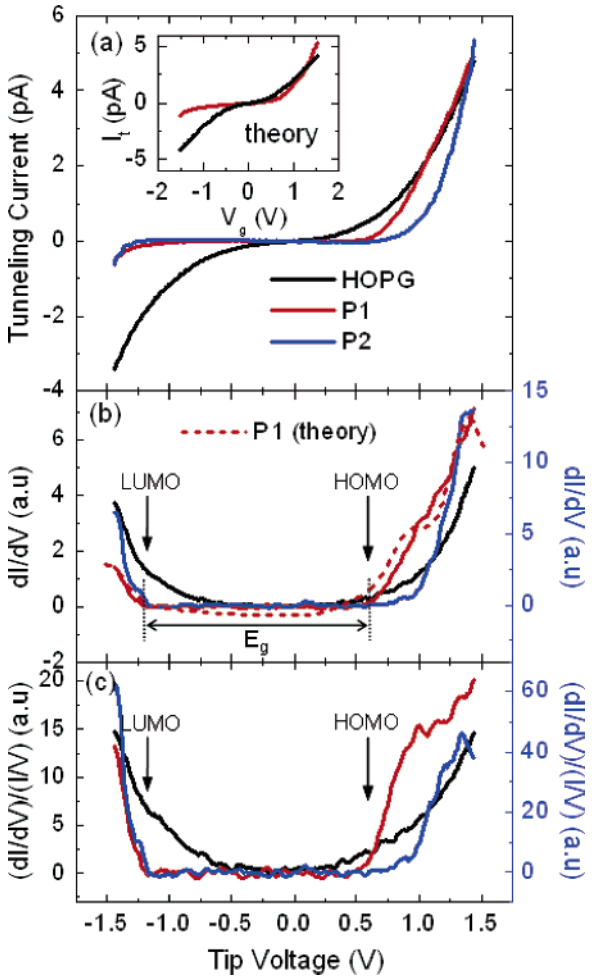

Figure 2. Experimental and calculated STS spectra. (a) Experimental $I-V$ curves recorded during a CITS measurement (topographic regulation set point: $I_t = 4.6$ pA, $V_g = 1.42$ V) over the bare substrate (HOPG, black), the first polymer monolayer (P1, red) and the second polymer layer (P2, blue). Calculated curves for the bare substrate and polymer monolayer are shown in the inset. (b) Conductance d*I*/d*V* spectra (solid lines) acquired with a lock-in amplifier. Note that an independent *Y*-scale has been used for P2 (right axis in blue), while HOPG and P1 curves share a common *Y*-scale (left axis, black). The dotted red line is the derivative of the polymer monolayer calculated $I-V$ (its *Y*-scale has been adjusted to the experimental curve). (c) Normalized conductance spectra. Arrows in (b) and (c) pinpoint the edges of HOMO and LUMO bands.

$I-V$ curves as well as topographic and spectroscopic images (Figure 2 and Figure 3, respectively) have been acquired between −1.44 and 1.44 eV for a deeper analysis of the polymer electronic states. $I-V$ curves and corresponding (d*I*/d*V*)s recorded over HOPG are consistent with the semimetallic nature of graphite. A totally different behavior is found for the polymer, resulting in a sharp spectroscopic contrast on CITS images within a broad energy range **(**Figure 3**)**. Both $I-V$ curves and conductance spectra exhibit an extended plateau (or conductance gap) with zero current. No negative differential resistance peaks are observed, in agreement with the general assumption that electronic delocalization occurs along the polymer backbone,[19,28] inducing a quasi-continuum of electronic states. Another remarkable feature of these spectra is their asymmetry, a much higher current being obtained for positive than for negative voltages.

Recently, Terada et al. have demonstrated that for poly(3-hexylthiophene) on silicon,[28,29] a valence-band-based conduction takes place whatever the bias voltage polarity. For P3DDT on HOPG, the STS conductance gap is however more probably related to the HOMO−LUMO band gap, as

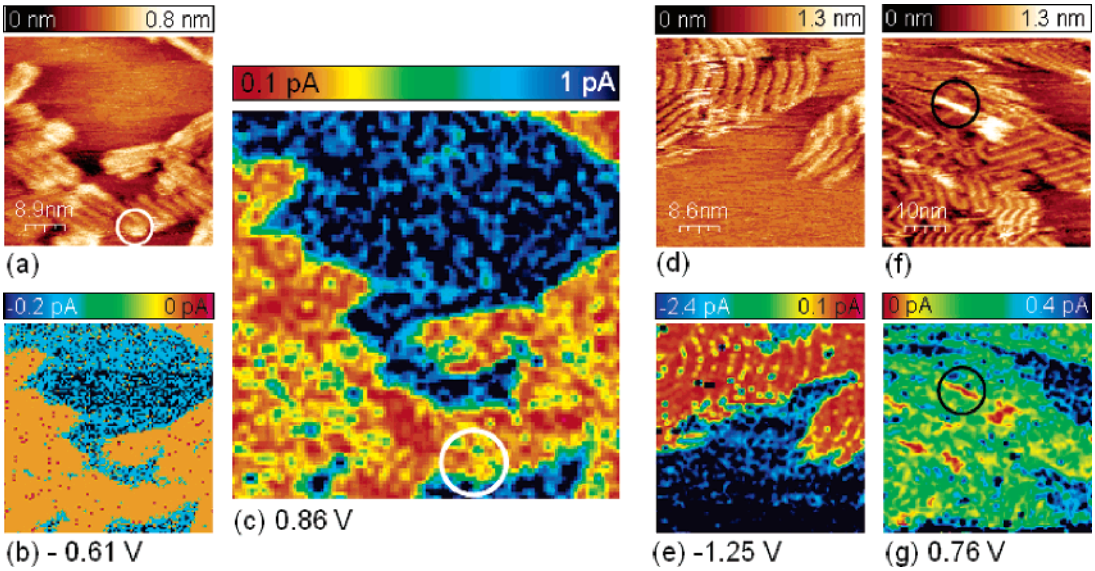

Figure 3. Topographic (300 × 300 pixels) and current (100 × 100 pixels) images acquired during three different CITS measurements. (a) Topographic STM image (50 nm × 50 nm) recorded with $I_t = 3.9$ pA, $V_g = 1.21$ V. Note that this image is almost free from "distortion" effects. (b, c) Current images acquired simultaneously with (a). Image (b) corresponds to electronic states within the polymer midgap. The location of a chain fold is highlighted by white circles in (a) and (c). (d) Topographic STM image (43 nm × 43 nm) recorded with $I_t = 4.1$ pA, $V_g = 1.45$ V. (e) Current image acquired simultaneously with (d) and resolving polymer chains. (f) Topographic STM image (50 nm × 50 nm) recorded with $I_t = 4.3$ pA, $V_g = 1.51$ V, filtered by a Gaussian smooth. (g) Current image acquired simultaneously with (f). Chains of the second layer are identified by black circles in (f) and (g). NB: the distortion in (d) and (e) and (f) and (g) images is due to thermal drift effects during the CITS acquisition.

previously demonstrated for polydiacetylene on the same substrate.[19] In that case, if existing, contrasts in CITS images at selected energies will directly reflect the effect of the local conformation on the polymer local semiconducting gap. However, with regard to the complexity of the substrate−polymer−tip junction, the interpretation of STS data remains delicate. To confirm the nature of the STS conductance gap and the positioning of the molecular levels, we have performed extensive simulations presented hereafter.

The STS spectra have been calculated using the elastic scattering formalism expressed within the tight binding approximation.[34,35] For P3DDT, physisorption on HOPG should not dramatically affect the macromolecule electronic properties, and in that case self-consistency is not mandatory to calculate the tunneling current. For the sake of accuracy, the electronic structure of the polymer has however been calculated using a self-consistent tight binding method described in refs 36 and 37.

Moreover, electronic correlations can strongly modify the molecular energetic levels. Electron−electron interactions (self-energy effects) inside the polymer and screening effects by the metallic electrodes have been henceforth taken into account. Then, ab initio calculations have been performed to provide an accurate description of the electronic properties of the system. The idea is to determine self-energy and screening effects from *first principle* calculations and to incorporate them into the tight binding scheme.

The effects of adsorption on P3DDT electronic properties have first been simulated in the frame of ab initio density functional theory using the generalized gradient spproximation for describing the exchange-correlation effects as implemented in the VASP code.[38] The band structure obtained for the one-dimensional periodic system (polymer physisorbed on graphene, inset of Figure 4a) did not show major modification compared to the one of the isolated molecule, except the alignment of the molecule midgap with graphite Fermi level (Figure 4a). This suggests that no significant charge transfer from the substrate should be expected and also justifies separate calculations for the polymer electronic structure. The tight binding molecular levels have just to be shifted and then to reproduce the proper positioning with respect to the Fermi level of the surface.

Under current flow from the tip to the surface, the molecule goes through a transition state that amounts to the injection of one extra charge (one electron or one hole) to one of the molecular states. The energies of the transition levels (labeled $\epsilon_i^{e(h)}(V_g)$) differ from the corresponding molecular levels' ones by quantities that are called self-energies.[39] The relevant gap for STM simulation becomes subsequently the so-called quasi-particle (QP) gap E_g^{qp} defined by the difference between the electronic affinity (EA) and the ionization potential (IP) of the molecule which corresponds to the injection of one electron to the LUMO or one hole to the HOMO of the molecule, respectively. These levels can easily be obtained from ab initio total energy calculations by

$$\begin{aligned} \mathrm{EA} &= E(-1) - E(0) \\ \mathrm{IP} &= E(0) - E(+1) \\ E_g^{qp} &= \mathrm{EA} - \mathrm{IP} \end{aligned} \tag{1}$$

where $E(-1)$, $E(0)$, and $E(+1)$ are the total energies of the negatively charged, neutral, and positively charged species, respectively.

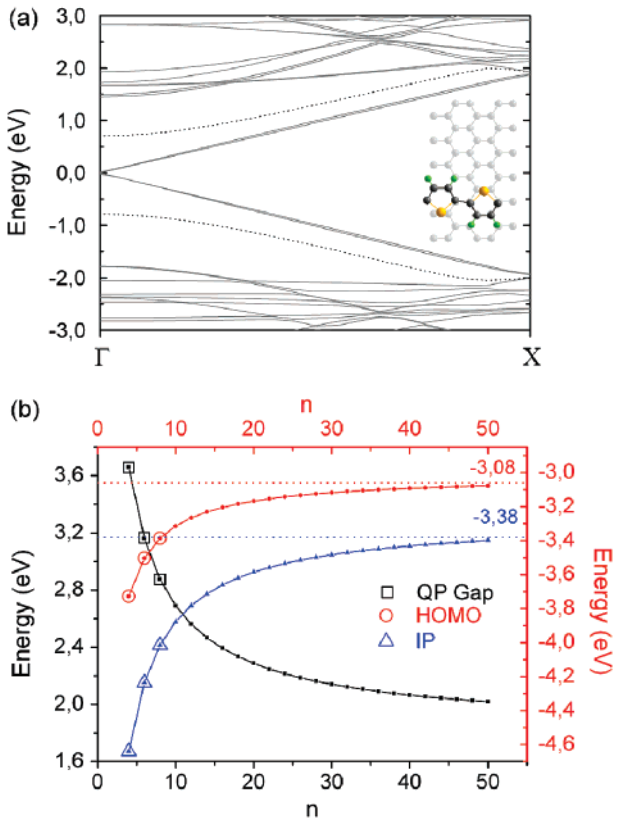

Figure 4. (a) Band structure of infinite poly(thiophene) on a graphene surface. The dotted lines identify the HOMO and LUMO of the polymer. Inset: relaxed periodic structure (polymer + surface) used for the band structure calculation. (b) (left axis) Evolution of the calculated quasi-particle gap (EA-IP) as a function of the number of rings (■) and the corresponding fitting curve. (right axis) Evolution of the HOMO (●) and IP (▲) levels as a function of the number of rings and their corresponding fitting curves. Calculated values have been fitted by a function $a_1 + a_2/n + a_3$, where a_1, a_2, and a_3 are fitting parameters and n is the number of tiophene rings.

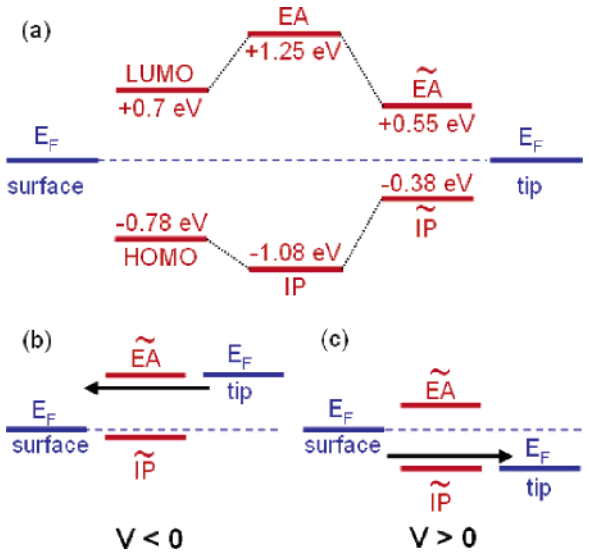

Figure 5. (a) Energy levels of octadecathienyl molecule with respect to the Fermi levels of the electrodes at zero bias: single-particle levels for the HOMO and LUMO, ionization levels corresponding to charging the molecule with one electron (EA) or one hole (IP) for the isolated molecule and for the molecule coupled to the electrodes (EÃ and IP̃, respectively). (b, c) Evolution of the bias-dependent molecular level positions taking $\eta = 0.33$ (see text): for a high enough negative bias, electrons are injected from the tip to the surface via EÃ the level of the molecule, whereas for a sufficiently positive bias electrons are injected from the surface to the tip via the IP̃ level of the molecule.

To incorporate self-energy effects in the TB scheme and to determine a realistic number of the polymer repeating units for the modeling, the next step is to investigate the evolution of the QP gap as a function of the number of thiophene cycles in the molecule (Figure 4b).

The simulated QP gap saturates from 18 units, the number of thiophene cycles for which it reaches ca. 2.3 eV. This is consistent with the "optical gaps" measured in P3ATs solutions,[40] whose values are indeed near to the QP ones, due to relatively low exciton energies for long enough π-conjugated macromolecules. The simulated value for longer chains is slightly smaller and reaches ca. 2 eV for 50 thiophene units. However, it is known that local approximations in the DFT theory (such as LDA or GGA) would underestimate QP gaps[41] defined as eq 1 for very long molecules. Moreover, a saturation of the optical gap above about 18 cycles has been already reported for other linear oligothiophenes.[42] Compared to the value measured for our P3DDT sample in solution (2.2 ± 0.1 eV from UV−vis spectroscopy), the simulated value obtained for 18 thiophene cycles appears then reasonable and the infinite long polymer chain has accordingly been replaced, for the following STM simulations, by this finite sized molecule while keeping the proper QP gap. It is also noteworthy that these 18 units statistically correspond to the shortest chains of our sample, and gap saturation above this size is therefore consistent with the absence of chain length dependent contrast on both topographic and spectroscopic images.

Noticeably, for a large number of rings, the difference between the IP and HOMO levels of the isolated molecules (plotted as a function of the number of thiophene rings in Figure 4b) displays a downward shift of 0.3 eV. This value corresponds to the self-energy that results from the injection of one extra charge within an occupied state of the molecule. Considering that the same effect occurs when the polymer is adsorbed on the surface, all the occupied states of the molecule have been shifted by 0.3 eV for a proper positioning of the IP level. A scissor operator has finally been applied to all unoccupied levels to set the quasi-particle gap of the polymer. The energetic scheme resulting from these self-energy effects is represented in Figure 5.

Next, screening effects have been taken into account by the image charge method,[37] leading to a reduction (in absolute value) of all molecular levels by 0.7 eV as depicted in Figure 5 ("screened" EA and IP will be referred hereafter as EÃ and IP̃, respectively). Here, we underline the importance of the screening by the metallic electrodes, as it counteracts self-energy effects by reducing the effective gap.

Finally, the dependence of the molecular transition levels with the applied bias has been described by[28,43]

$$\epsilon_i^{e(h)}(V_g) = \epsilon_i^{e(h)}(V_g{=}0) - (1 - \eta)eV_g \qquad (2)$$

where η is the same constant for all levels.

A very good agreement between the measured and calculated spectra has been reached by adjusting the parameter η to 0.33, which is consistent with both the relatively large tip−sample distance implied by STM operations in the low current mode and a low macromolecule−substrate interaction.[28,43] Remarkably, within the band gap, the density of states takes no finite value, leading to a zero gap of ca. $E_g = 1.7$ eV from experimental dI/dV and normalized (dI/dV)/(I/V) curves (see Figure 2b,c), in good agreement with the simulations. Similarly to the case of polythiophenes on I−Au(111),[22] this last value is smaller than the gap obtained by other probes for P3ATs samples in solutions. Here, as explained previously, the modeling clearly establishes the origin of this difference. The optical gap probed in solution is indeed very near to the quasi-particle gap, while "extrinsic" screening effects within the tunneling junction reduce the effective gap measured by STS.

It also clearly appears from the modeling that, depending on the bias polarization, electron will transit, as depicted in Figure 5, through asymmetrically positioned I$\tilde{P}$ and E$\tilde{A}$ levels, related to HOMO and LUMO molecular levels, leading to an asymmetric spectrum. This definitely confirms the relation between the STS conductance gap and the polymer semiconducting band gap and, moreover, accounts for the rectifying shape displayed by $I-V$ curves.

Accordingly to the STS spectra, the absence of electronic states within the gap is also evidenced from low bias 2D CITS images (Figure 3b), for which the current is almost perfectly constant at zero level within our resolution limit (a few tens of femtoampere). Besides the aforementioned absence of charge transfer effects from the HOPG substrate, this shows that in our case, there is most probably no injection of charge-carrying polarons by the STM tip into the polymer. For P3DDT on HOPG, there is henceforth no evidence for spatially dependent partial or total gap closure effects similar to the one reported by Akai-Kasaya et al. in the case of PDA.[19,20] Such an absence of localized polarons (at least at the time scale of our experiment) is also fully consistent with our topographic images, which display no specific contrast such as "bright spots" specifically localized on chain segments.[21] So far, such spots have been only observed for polythiophenes on the I−Au(111) surface,[21] where the iodine is more likely to locally oxidize the polymer chains.

In a search of specific contrast associated to chain folds on CITS images, we now focus on energy ranges corresponding to HOMO (parts c and g of Figure 3) and LUMO bands (Figure 3e). Over the polymer monolayer, the tunneling current remains constant within statistical fluctuation whatever the applied bias voltage, and no noticeable correlation between local topological features and the variations of the HOMO−LUMO gap can be detected. An increase of the HOMO−LUMO gap over chain folds could be expected due to a weakened overlap between thiophenes π-orbitals within the fold. However, the spectroscopic measurements presented here bring direct evidence that the electronic properties of a single chain are weakly affected by folding at 300 K. Considering the thermal broadening effects, one can reasonably deduce from our STS measurements that the increase in the HOMO−LUMO gap over folds does not exceed a few tens of millielectronvolt. This somehow surprising result is more understandable if one compares the P3DDT case with other model systems. For instance, for an oligo**(**thiophene**)** macrocycle **(**C18T**)**, an optical band gap[42] of $E_g = 2.959$ eV has been measured while a slightly smaller value has been reported for the linear 19T oligo(thiophene) with a very close length, $E_g = 2.883$ eV. As P3DDT folds exhibit similar curvature radius as the ones reported for C18T, one may tentatively extrapolate the former results to the polymer case. The aforementioned studies on oligo(thiophene)s support the idea that the local gap variation may be limited to a few tens of millielectronvolt over chain folds and will henceforth remain hidden for STS at room temperature.

While chain folds seem to impact weakly on the polymer electronic properties, a remarkable spectroscopic contrast is obtained on CITS images recorded over chains of the second layer for energies above +0.6 eV (Figure 3g), which corresponds to the edge of the monolayer HOMO band. Spectra recorded over the monolayer and second layer display common features, with a net zero gap between HOMO and LUMO edges. The contrast above P2 arises from a 0.3 eV shift of HOMO's falling edge, leading to a wider zero conductance gap of ca. $E_g = 2$ eV (see Figure 2b). It is noteworthy that besides this gap widening, dI/dV spectra above P2 display higher values those over P1 for bias value corresponding to the set point for topographic imaging, which agrees with the above-mentioned larger h_{P2-P1} stacking value extracted from topographic images in the constant current mode. On the other hand, this apparent increase of the effective gap is striking, as a diminution is generally expected for such polymer configuration. The stacking of π-conjugated molecules on top of each other is indeed usually supposed to involve an interlayer overlap of π-orbitals or "π-stacking", more favorable to electronic delocalization than intrachain orbital overlap. The situation of P3DDT bilayers appears then rather different from the one reported for bis(urea)-substituted thiophene derivatives,[6] for which the zero STS conductance gap was reported to be reduced over self-assembled ribbons of "π-stacked" oligomers. Here, we underline that P3DDT self-assembly on HOPG also differs from the one displayed by the former oligomers, for which the thiophenes rings are tilted[6] with respect to the surface, while P1 π-conjugated cycles lie almost flat on the surface.

As suggested previously, in the case of P3DDT, disorder effects may dramatically affect the $\pi-\pi$ interaction. Anomalous torsion angles between P2 adjacent thiophene rings would damage not only the overlap of π-orbitals from one layer to the other but also intrachain overlap within P2 π-conjugated backbones, as shown by calculations for poly(thiophene)s[44] and other materials.[45]

Other effects are however likely to play a role in the modifications of the effective STM conductance gap. Po-

larization effects especially need to be considered as the electrical environment of P2 chains is different from P1 ones. More precisely, charges in isolated chains of the second layer cannot be screened efficiently by neighboring macromolecules,[46] while screening effects occur mainly for the underlying P3DDT monolayer, whose polarization constant is much lower than that for HOPG. Such effects have already been proposed by others to account for STS conductance gap variations on organic multilayers.[47] Again, we note the differences with the case of self-assembled ribbons of π-stacked thiophene derivatives. Indeed, the polarization effect should be relatively similar for isolated bis(urea)-substituted thiophene molecules and tilted self-assembled ribbons and should therefore not shadow the gap reduction generated by the π-stacking between thiophene cycles of these molecules.

Finally, the case of P3DDT seems to remain somehow open, as conformational and polarization effects are likely to simultaneously contribute to the STS conductance gap. However, as the same gap increase has been detected on several P2 chains in this study, we suggest that the effective gap variation is indeed in majority dominated by polarization effects.

In conclusion, we have demonstrated the possibility to address directly the relation between local polymer conformation and electronic properties of self-organized regioregular poly(3-alkylthiophene)s by 2D STS imaging. With the support of theoretical modeling, we have shown that the STS spectra recorded over the polymer are indeed related to its HOMO−LUMO band gap, without noticeable charge transfer from the underlying substrate. Compared to measurements in solutions, the apparent conductance gap reduction to ca. 1.7 eV has been accounted for by extrinsic screening effects in the tunneling junction. The homogeneity of P3DDT electronic properties probed by 2D spectroscopic images with a resolution down to the single polymer chain gives direct evidence that the HOMO−LUMO gap variation is at maximum limited to some tens of millielectronvolt over chain folds. On the other hand, the 0.3 eV increase of the measured zero gap over the partially nucleated second layer raises more questions. It will be essential to definitely establish if this phenomenon is due to disorder effects within the second polymer layer or if as we propose polarization effects dominate the local variations of the STS effective conductance gap on polymer layers. Cryogenic 2D STS measurements are the next step to address these issues, as they combine a better stability for ultimate topographic resolution with a higher energy resolution.

Acknowledgment. This work has been supported by the French Ministry of Research under the grant "RTB: Post CMOS moléculaire 200 mm". A. Rubio is supported by the Nanoquanta Network of Excellence **(**NMP4-CT-2004-500198**)**, Spanish MCyT, and the Humboldt Foundation under the 2005 Bessel Award.

References

(1) Yokoyama, T.; Yokoyama, S.; Kamikado, T.; Okuno, Y.; Mashiko, S. *Nature* **2001**, *413*, 619.
(2) Qiu, X. H.; Nazin, G. V.; Ho, W. *Phys. Rev. Lett.* **2004**, *93*, 196806.
(3) Iancu, V.; Deshpande, A.; Hla, S.-W. *Nano Lett.* **2006**, *6*, 820.
(4) Yanagi, H.; Ikuta, K.; Mukai, H.; Shibutani, T. *Nano Lett.* **2002**, *2*, 951.
(5) Grill, L.; Rieder, K.-H.; Moresco, F.; Stojkovic, S.; Gourdon, A.; Joachim, C. *Nano Lett.* **2005**, *5*, 859.
(6) Gesquière, A.; De Feyter, S.; De Schryver, F. C.; Schoonbeek, F.; van Esch, J.; Kellogg, R. M.; Feringa, B. L. *Nano Lett.* **2001**, *1*, 201.
(7) Mena-Osteritz, E. *Adv. Mater.* **2002**, *14*, 609.
(8) Gesquière, A.; Jonkheijm, P.; Hoeben, F. J. M.; Schenning, A. P. H. J.; De Feyter, S.; De Schryver, F. C.; Meijer, E. W. *Nano Lett.* **2004**, *4*, 1175.
(9) Joachim, C.; Gimzewski, J. K.; Aviram, A. *Nature* **2000**, *408*, 541.
(10) Lu, X.; Grobis, M.; Khoo, K. H.; Louie, S. G.; Crommie, M. F. *Phys. Rev. B* **2004**, *70*, 115418.
(11) Grobis, M.; Wachowiak, A.; Yamachika, R.; Crommie, M. F. *Appl. Phys. Lett.* **2005**, *86*, 204102.
(12) Pradhan, N. A.; Liu, N.; Silien, C.; Ho, W. *Nano Lett.* **2005**, *5*, 55.
(13) Mena-Osteritz, E.; Bäuerle, P. *Adv. Mater.* **2006**, *18*, 447.
(14) Kim, P.; Odom, T. W.; Huang, J.-L.; Lieber, C. M. *Phys. Rev. Lett.* **1999**, *82*, 1225.
(15) Czerw, R.; Terrones, M.; Charlier, J.-C.; Blase, X.; Foley, B.; Kamalakaran, R.; Grobert, N.; Terrones, H.; Tekleab, D.; Ajayan, P. M.; Blau, W.; Rühle, M.; Carroll, D. L. *Nano Lett.* **2001**, *1*, 457.
(16) Odom, T. W.; Huang, J.-L.; Lieber, C. M. *J. Phys.*: *Condens. Matter* **2002**, *14*, R145.
(17) Okawa, Y.; Aono, M. *Nature* **2001**, *409*, 683.
(18) Okawa, Y.; Aono, M. *J. Chem. Phys.* **2001**, *115*, 2317.
(19) Akai-Kasaya, M.; Shimizu, K.; Watanabe, Y.; Saito, A.; Aono, M.; Kuwahara, Y. *Phys. Rev. Lett.* **2003**, *91*, 255501
(20) Akai-Kasaya, M.; Yamamoto, Y.; Saito, A.; Aono, M.; Kuwahara, Y. *Jpn. J. Appl. Phys.* **2006**, *45*, 2049.
(21) Sakaguchi, H.; Matsumura, H.; Gong, H. *Nat. Mater.* **2004**, *3*, 551.
(22) Sakaguchi, H.; Matsumura, H.; Gong, H.; Abouelwafa, A. M. *Science* **2005**, *310*, 1002.
(23) Aasmundtveit, K. E.; Samuelsen, E. J.; Guldstein, M.; Steinsland, C.; Flornes, O.; Fagermo, C.; Seeberg, T. M.; Pettersson, L. A. A.; Inganäs, O.; Feidenhans'l, R.; Ferrer, S. *Macromolecules* **2000**, *33*, 3120.
(24) Derue, G.; Coppée, S.; Gabriele, S.; Surin, M.; Geskin, V.; Monteverde, F.; Leclère, P.; Lazzaroni, R.; Damman, P. *J. Am. Chem. Soc.* **2005**, *127*, 8018.
(25) Sirringhaus, H.; Brown, P. J.; Friend, R. H.; Nielsen, M. M.; Bechgaard, K.; Langeveld-Voss, B. M. W.; Spiering, A. J. H.; Janssen, R. A. J.; Meijer, E. W.; Herwig, P.; de Leeuw, D. M. *Nature* **1999**, *401*, 685.
(26) Ong, B. S.; Wu, Y.; Liu, P.; Gardner, S. *J. Am. Chem. Soc.* **2004**, *126*, 3378.
(27) Terada, Y.; Choi, B.-K.; Heike, S.; Fujimori, M.; Hashizume, T. *Nano Lett.* **2003**, *3*, 527.
(28) Terada, Y.; Miki, K.; Fujimori, M.; Heike, S.; Suwa, Y.; Hashizume, T. *J. Appl. Phys.* **2005**, *97*, 124302.
(29) Terada, Y.; Shigekawa, H.; Suwa, Y.; Heike, S.; Fujimori, M.; Hashizume, T. *Jpn. J. Appl. Phys.* **2006**, *45*, 1956.
(30) Mena-Osteritz, E.; Meyer, A.; Langeveld-Voss, B. M. W.; Janssen, R. A. J.; Meijer, E. W.; Bäuerle, P. *Angew. Chem., Int. Ed.* **2000**, *39*, 2679.
(31) Brun M.; Demadrille, R.; Rannou, P.; Pron, A.; Travers, J.-P.; Grévin, B. *Adv. Mater*. **2004**, *16*, 2087.
(32) Prietsch, M.; Samsavar, A.; Ludeke, R. *Phys. Rev. B* **1991**, *43*, 11850.
(33) Grévin, B.; Rannou, P.; Payerne, R.; Pron, A.; Travers, J.-P. *J. Chem. Phys.* **2003**, *118*, 7097.
(34) Delerue, C.; Lannoo, M. *Nanostructures: Theory and Modeling*; Springer-Verlag: Berlin, Heidelberg, 2004.
(35) Dubois, M.; Delerue, C.; Allan, G. *Phys. Rev. B* **2005**, *71*, 165435.
(36) Krzeminski, C.; Delerue, C.; Allan, G.; Haguet, V.; Stiévenard, D.; Frère, P.; Levillain, E.; Roncali, J. *J. Chem. Phys.* **1999**, *111*, 6643.
(37) Krzeminski, C.; Delerue, C.; Allan, G. *J. Phys. Chem. B* **2001**, *105*, 6321.
(38) http://cms.mpi.univie.ac.at/vasp/. Kresse, G.; Furthmüller, J. *Phys. Rev. B* **1996**, *54*, 11169.
(39) Niquet, Y. M.; Delerue, C.; Allan, G.; Lannoo, M. *Phys. Rev. B* **2002**, *65*, 165334.
(40) Schilinsky, P.; Asawapirom, U.; Scherf, U.; Biele, M.; Brabec, C. J. *Chem. Mater.* **2005**, *17*, 2175.

(41) van Faassen, M.; de Boeij, P. L.; van Leeuwen, R.; Berger, J. A.; Snijders,. J. G. *Phys. Rev. Lett.* **2002**, *88*, 186401.
(42) Bednarz, M.; Reineker, P.; Mena-Osteritz, E.; Bäuerle, P. *J. Lumin.* **2004**, *110*, 225.
(43) Krzeminski, C.; Delerue, C.; Allan, G.; Vuillaume, D.; Metzger, R. M. *Phys. Rev. B* **2001**, *64*, 085405.
(44) Brédas, J. L.; Street, G. B.; Thémans, B.; André, J. M. *J. Chem. Phys.* **1985**, *83*, 1323.
(45) Miao, M. S.; Van Camp, P. E.; Van Doren, V. E.; Ladik, J. J.; Mintmire, J. W. *J. Chem. Phys.* **1998**, *109*, 9623.
(46) Hill, I. G.; Mäkinen, A. J.; Kafafi, Z. H. *J. Appl. Phys.* **2000**, *88*, 889.
(47) Tsiper, E. V.; Soos, Z. G.; Gao, W.; Kahn, A. *Chem. Phys. Lett.* **2002**, *360*, 47.

NL061018W